Eur. Phys. J. D **55**, 379–389 (2009)
DOI: 10.1140/epjd/e2009-00149-x

THE EUROPEAN PHYSICAL JOURNAL D

Regular Article

Signatures of the Unruh effect via high-power, short-pulse lasers

P.G. Thirolf[1,a], D. Habs[1,2], A. Henig[1], D. Jung[1], D. Kiefer[1], C. Lang[1], J. Schreiber[1,3], C. Maia[4], G. Schaller[5], R. Schützhold[4], and T. Tajima[1]

[1] Faculty of Physics, Ludwig-Maximilians-University München, 85748 Garching, Germany
[2] Max-Planck Institute of Quantum Optics, 85748 Garching, Germany
[3] Imperial College, SW7 2AZ London, UK
[4] Fachbereich Physik, University of Duisburg-Essen, 47048 Duisburg, Germany
[5] Institut für Theoretische Physik, TU Berlin, 10623 Berlin, Germany

Received 14 November 2008 / Received in final form 28 February 2009
Published online 16 May 2009 –

Abstract. The ultra-high fields of high-power short-pulse lasers are expected to contribute to understanding fundamental properties of the quantum vacuum and quantum theory in very strong fields. For example, the neutral QED vacuum breaks down at the Schwinger field strength of 1.3×10^{18} V/m, where a virtual e^+e^- pair gains its rest mass energy over a Compton wavelength and materializes as a real pair. At such an ultra-high field strength, an electron experiences an acceleration of $a_S = 2 \times 10^{28} g$ and hence fundamental phenomena such as the long predicted Unruh effect start to play a role. The Unruh effect implies that the accelerated electron experiences the vacuum as a thermal bath with the Unruh temperature. In its accelerated frame the electron scatters photons off the thermal bath, corresponding to the emission of an entangled pair of photons in the laboratory frame. While it remains an experimental challenge to reach the critical Schwinger field strength within the immediate future even in view of the enormous thrust in high-power laser developments in recent years, the near-future laser technology may allow to probe the signatures of the Unruh effect mentioned above. Using a laser-accelerated electron beam ($\gamma \sim 300$) and a counter-propagating laser beam acting as optical undulator should allow to create entangled Unruh photon pairs (i.e., signatures of the Unruh effect) with energies of the order of several hundred keV. An even substantially improved experimental scenario can be realized by using a brilliant 20 keV photon beam as X-ray undulator together with a low-energy ($\gamma \approx 2$) electron beam. In this case the separation of the Unruh photon pairs from background originating from linearly accelerated electrons (classical Larmor radiation) is significantly improved. Detection of the Unruh photons may be envisaged by Compton polarimetry in a 2D-segmented position-sensitive germanium detector.

PACS. 04.62.+v Quantum fields in curved spacetime – 12.20.Fv Experimental tests – 41.60.-m Radiation by moving charges – 42.50.Dv Quantum state engineering and measurements

1 Introduction

The development of stable, ultra high intensity lasers has led to a renewed interest in strong field effects in quantum electrodynamics (QED). Examples include the search for long sought phenomena, such as the Schwinger pair production mechanism [1], which is a non-perturbative QED vacuum process. Another quantum field theory prediction that may benefit from new experimental techniques is the Unruh effect [3]. Given the vacuum state experienced by inertial (Minkowski) observers, it has been shown [3] that uniformly accelerated (Rindler) observers with proper acceleration a will experience such state as a thermal bath of particles at the Unruh temperature

$$kT_U = \frac{\hbar a}{2\pi c}, \tag{1}$$

see Figure 1. Even though the presence of $\hbar/c$ necessitates an acceleration as great as $a \geq 10^{20} g$ (with g being the earth's surface gravity) in order to produce a reasonable Unruh temperature, the striking implication it draws is that the particle content of quantum field theory is an observer dependent property. Furthermore, the Unruh effect is closely related via the equivalence principle to another well known predicted phenomenon: the Hawking radiation of black holes [4], characterized by the black-body Hawking temperature

$$kT_H = \frac{\hbar c^3}{8\pi GM} = \frac{\hbar g_s}{2\pi c}, \tag{2}$$

where g_s is the black hole surface gravity. As simple as this equation for the thermal Hawking radiation may appear, one should note that it combines fundamental quantities from four seemingly disparate fields of physics:

[a] e-mail: Peter.Thirolf@physik.uni-muenchen.de

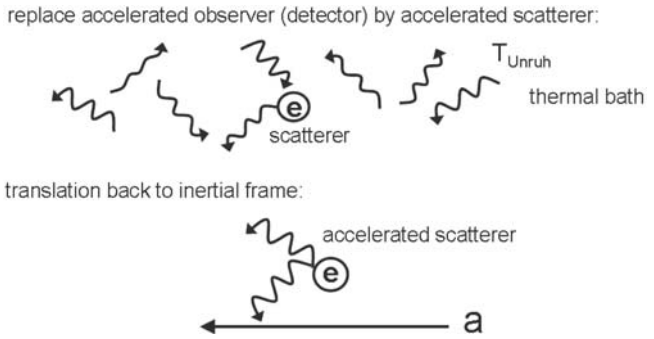

Fig. 1. Schematical illustration of the creation of entangled photon pairs (Unruh photons) in the laboratory frame via non-inertial scattering of virtual photons off an accelerating scatterer.

gravity (G), quantum mechanics ($\hbar$), relativity (c), and thermodynamics (k). Thus equation (2) acts as a bridge, indicating the interplay between (quantum) gravity and thermodynamics (e.g., black hole entropy). Perhaps our situation today is comparable to the early 1920s, when the theoretical description of the just discovered Compton effect was formulated within a semi-classical framework prior to the development of quantum mechanics. For both, the Unruh effect and the Hawking effect, a uniform acceleration is not an essential ingredience.

An intuitive way to understand equation (2) is by means of the horizon experienced by accelerated observers, represented by the light-cone drawn in Figure 2. Such observers will experience the space-time region (the left Rindler wedge) beyond the light-cone (the horizon) as a non-accessible one, in the same sense as outside observers of a black hole can not access the region beyond the horizon located at the Schwarzschild radius $R_{\rm Sch} = 2GM/c^2 = c^2/2g_s$. In the case of accelerated observers, their (minimal) distance to the horizon will be given by (cf. Fig. 2)

$$d = \frac{c^2}{a}, \tag{3}$$

and the thermal bath they experience is similar to the one experienced by stationary observers of a black hole who detect emission of Hawking radiation[1]. It is important to remark that there is no contradiction between the different particle contents experienced by Minkowski and Rindler observers. In the same way as the energy in classical mechanics is consequence of a natural time translation symmetry, in quantum field theory the energy, and hence the frequency, associated to each field mode is inherent to their time translation symmetry. Since inertial and accelerated observers follow different time-like Killing vectors, i.e., their clocks experience different natural (proper) times, they differ in their particle definition. In what follows a "Rindler photon" is the one defined with respect to (uniformly) accelerated observers, while a "Minkowski photon" is the usual one defined with respect to inertial observers.

[1] The reason for this similarity relies on the fact that the black-hole metric can be well approximated by the Rindler line element near the horizon $r \approx R_{\rm Sch}$.

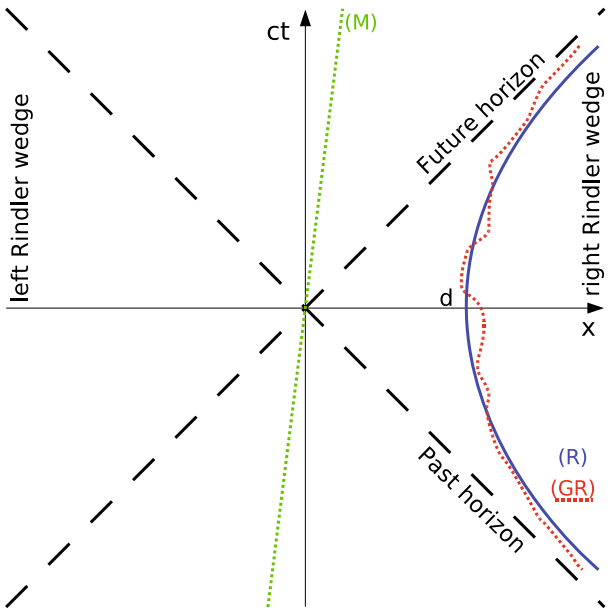

Fig. 2. (Color online) World-lines of an intertial, i.e., Minkowski (M), observer (straight green line) and a Rindler (R) observer (solid blue curve) undergoing uniform acceleration. The horizons mark the borders of the left and right Rindler wedges and are depicted by black dashed lines. Another trajectory (wiggly red dotted curve) corresponding to a non-uniform acceleration (GR) still lies within the right Rindler wedge and hence the horizon concept does also apply here. This more general observer (GR) would not experience the Minkowski vacuum as a purely thermal bath – but still as an excited state with a non-vanishing entropy.

1.1 Signatures of the Unruh effect

A possible way to bypass the difficulty to maintain the necessary acceleration for an Unruh detector is to replace it by an accelerated scatterer, e.g. an electron. The implications of doing so may be best appreciated in the accelerated frame comoving with the electron. According to the Unruh effect, the electron experiences a thermal bath of (Rindler) photons with which it interacts by scattering, as depicted in Figure 1. As shown in [5] and further discussed below, the translation back to the inertial frame of this process means that for each scattering event of (Rindler) thermal photons, as viewed in the co-accelerated frame, corresponds an emission of two (Minkowski) photons as viewed in the inertial/laboratory frame. Furthermore, this pair of photons will be entangled, and presenting properties that may be used to clearly distinguish it from the background of classical Larmor radiation also emitted in the laboratory frame due to the electron acceleration. For brevity, the entangled pair of (Minkowski) photons emitted due to the process described above – which can conveniently be understood in terms of the Unruh effect – will henceforth be called "Unruh radiation" or "Unruh photons" in order to differentiate them from the classical Larmor background. Note that they are still Minkowski photons and should not be mistaken for the Rindler photons defined in the co-accelerated frame.

A useful picture to understand the above results is the following: as shown by Unruh and Wald [7], to every (Rindler) photon absorbed by an accelerated detector, as viewed in the co-accelerated frame, a corresponding (Minkowski) photon will be emitted in the inertial frame. This becomes obvious after realizing that the initial Minkowski vacuum is the ground state (in the inertial frame) and thus any alteration of the quantum state by such an accelerated detector can only imply an excitation, i.e., photon creation, for inertial observers. When replacing the detector by a scatterer, like an electron, it is reasonable that the scattering process, viewed in the co-moving frame as emission and subsequent absorption (i.e., *two* processes) of a (Rindler) photon, implies the emission of *two* (Minkowski) photons as viewed in the laboratory frame. The entanglement of the pair of Unruh photons can also be understood in this picture: in the co-accelerated frame, the absorbed and the re-emitted Rindler photons have the same (Rindler) frequency $\omega_{\rm in}^{\rm (Rind)} = \omega_{\rm out}^{\rm (Rind)}$ as well as the same linear polarization. As a result, the pair of Unruh photons is naturally created in an entangled (squeezed) state.

As easy as it is to accelerate electrons, it is still non-trivial to maintain a sufficiently large and uniform acceleration for a long enough period of time. Therefore, a more realistic scenario, as described in [6], consists of the analysis of electrons subject to oscillatory motion, e.g., in an undulator field. Even though it implies slight changes to the above picture (e.g., the electron does no longer experience a purely thermal bath), the main mechanism remains correct and it remains true that Unruh photon pairs are created with their distinctive properties. In what follows we present possible experimental setups devised to differentiate and detect this characteristic Unruh radiation over the background of Larmor radiation.

1.2 Comparison with other approaches

It is interesting to notice that the classical Larmor radiation can also be understood from the point of view of the co-accelerated frame [8,9], where it corresponds to a specific class of the (Rindler) photons present in the thermal bath, namely the zero-energy Rindler modes, i.e., photons of zero Rindler frequency $\omega^{\rm (Rind)}$ but non-zero transverse momentum $k_\perp$. Since in this case their absorption and emission process, as viewed in the co-accelerated frame, is subject to $\omega_{\rm in}^{\rm (Rind)} = \omega_{\rm out}^{\rm (Rind)} = 0$, the emitted photons as viewed in the Minkowski frame will not be entangled (their polarization is fixed by the acceleration direction) and we naturally recover the fact that Larmor radiation is incoherent.

Of course, it is always possible to describe any given process in both frames (inertial and non-inertial) correctly. For example, experiments performed on a carrousel can either be explained in the co-rotating frame using centrifugal and Coriolis forces or in the inertial frame. However, the level of complexity of the description and the resulting understanding can be very different. To our opinion, the classical Larmor radiation can best be understood in the inertial frame – whereas the accelerated frame provides the most suitable and natural description for the entangled photon pair creation – which we therefore call Unruh radiation. Clearly, the entangled photon pairs could also be predicted, although in a more complicated way, by inertial observers after a third-order (three vertices) QED calculation [10]. However, the origin of the photon pairs and their entanglement is much harder to understand within this approach. In summary, the discussed experiments are as much or as little a verification of the Unruh effect as Foucault's pendulum proves the existence of the Coriolis force – but both experiments were/are worth doing, we think, in order to deepen our understanding of physics, especially when keeping in mind the equivalence of the Unruh effect and the Hawking effect.

1.3 Prior experimental settings

An interesting experiment where data was tentatively explained in terms of the Unruh effect is the spin-flip of electrons in storage rings. An initially unpolarized electron beam, trapped in a storage ring by a perpendicular magnetic field, tends to acquire spin polarization along the central axis direction, which is known as the Sokolov-Ternov effect. This polarization fails to be perfect, i.e. a minor component of the beam remains antiparallel ('spin down') instead of parallel ('spin up') to the magnetic field. Bell and Leinaas [11] have proposed to explain the beam's depolarization through the use of the Unruh effect, e.g. in the electron's co-accelerated frame the presence of a (approximately) thermal bath would induce thermal distributions between the up and down spin states of the electron, playing the role of a two-level Unruh detector. Nonetheless, a more realistic description of this process reveals that the population of up and down states clearly departs from being thermal (or even the approximate thermality expected from a circular trajectory). The reason for this lies in the importance of the electron's transverse degree of freedom in this setting, which implies that the Unruh effect, alone, does not directly explain the experimental data [9,12], i.e., only part of the depolarization can be understood via the Unruh effect.

It is also worth mentioning that our proposal presents marked similarities (the lowest-order Feynman diagrams are basically the same) with X-ray parametric down conversion in non-linear crystals, as envisaged by Freund and Levine [13] and realized by Eisenberger and MacCall [14] (see also [15,16] for similar experiments with synchroton radiation). There an incoming X-ray photon is split into a photon pair whose summed frequency matches the original photon, but whose wavevectors are correlated with the crystal lattice, granting coherence to the photon pair. Even though this effect could be interpreted as an analogous weak-field limit of the Unruh radiation discussed here (where the role of the laser-accelerated electrons is replaced by the atoms of the non-linear crystal), the picture of a nearly classical electron trajectory – which is crucial for the interpretation in terms of the Unruh effect – does not apply in this case.

Table 1. Correlation between laser intensity, electric field, electron acceleration, resulting Unruh temperatures and event horizon distances.

Method	I [W/cm^2]	E [V/m]	$\hbar\omega$ [eV]	a [g]	kT_{Unruh} [keV]	Horizon distance d
Laser focus	10^{23}	10^{15}	1	2×10^{25}	8×10^{-2}	0.5 nm
Coherent harmonic focusing	5×10^{29}	1.3×10^{18}	1	2×10^{28}	80	0.5 pm
Lorentz boost ($\gamma = 10^3$)	2×10^{36}	3×10^{21}	1	4×10^{31}	1.6×10^5	0.3 fm

2 Ultra high laser fields as a doorway to Unruh radiation

The most promising experimental approach to study the Unruh effect in the laboratory was proposed in 1999 by Chen and Tajima [17]. They suggested to use the interaction of a high-intensity laser field with an electron for testing quantum field theory in curved spacetime, especially to demonstrate the detection of Unruh radiation.

With the enormous progress in the development of high-intensity, short-pulse lasers in recent years the experimental approach to Unruh radiation has reached a stage where its detection can be envisaged within the next years. While e.g. for the terrestrial acceleration $a = g$ the resulting Unruh temperature $T_U = 4 \times 10^{-20}$ K $= 3.3 \times 10^{-24}$ eV/k_B will stay far below any experimentally accessible range, novel short-pulse, high-intensity lasers will allow to push T_U into an experimentally accessible regime. Two experimental scenarios will be presented in this section, the first one drawing from the availability of high-energy laser-accelerated electrons, while the second one will exploit brilliant X-ray photon beams presently being developed. In the first scenario (see Sect. 2.3) electrons accelerated to relativistic energies (<GeV) [19–23] within distances of only a few millimeters together with the technique of coherent harmonic focusing [25] of an optical laser serving as undulator can be used to probe vacuum fluctuations by the creation of Unruh photon pairs in the energy region of a few hundred keV. In the second scenario (see Sect. 2.4) the optical undulator will be replaced by a brilliant X-ray beam, while the electron beam energy will be reduced to e.g. 1 MeV. Also this scenario allows to create ultra high electric fields, accelerating electrons such that Unruh photon energies measurable with modern γ-spectroscopic techniques will be produced. The advantages of this scheme will be discussed in Section 2.4.

2.1 Creation of ultra high electrical fields

While presently existing high-power, short-pulse lasers in the multi-TW and even PW regime routinely reach intensities already between 10^{18}–10^{21} W/cm^2, upcoming laser facilities like the Petawatt Field Synthesizer (PFS) in Garching [24] will extend this to about 10^{22} W/cm^2 with the ultimate goal of the ELI project to realize an Exawatt laser system reaching a focused laser intensity of up to 10^{26} W/cm^2 within the next decade [18]. Table 1 gives a compilation of characteristic properties that follow from a given focused laser intensity I: electric field strength E, electron acceleration a (in units of the terrestrial acceleration g), Unruh temperature and event horizon distance $d = c^2/a$. The numbers are given for three different scenarios: in the first row a laser with a focused intensity of 10^{23} W/cm^2 is considered. In combination with the coherent focusing of high surface harmonics [25] the critical Schwinger field may be attainable with properties as listed in the middle row. Finally a situation is shown, where the Lorentz boost of a counterpropagating highly relativistic electron beam ($\gamma = 1000$) is used to boost the laser intensity in the rest frame of the electron by a factor of $I \times 4\ \gamma^2$, leading to the numbers listed in the bottom row. In this scenario the Unruh temperature would almost reach the value of the quark-gluon plasma phase transition at ≈170 MeV [26].

In the last column the corresponding values of the event horizon distances are given, which range from nm down to fractions of a fm.

2.2 Production of Unruh photons in ultra strong fields

As pointed out before, two theoretical studies have been performed in non-linear QED resulting in quantitative predictions of yields for Unruh radiation as well as for the dominant background contribution, which is given by the classical radiation of accelerated electrons (Larmor radiation) [5,6]. It should be mentioned that although formulated by Larmor already back in 1897, the classical Larmor radiation has so far never been experimentally identified for *uniform* acceleration.

In a first scenario with nearly constant proper electron acceleration, the probability for the emission of Unruh radiation scales with $P_{\mathrm{Unruh}} \sim (E/E_S)^4$ (where E_S denotes the critical or Schwinger field strength $E_S = 1.3 \times 10^{18}$ V/m), thus requiring extremely strong electrical laser-generated fields near the critical field, while the short pulse leads to a broad Larmor background spectrum [5]. In contrast, an arrangement exploiting an oscillating acceleration provided by an undulator or a counter-propagating laser beam results in $P_{\mathrm{Unruh}} \sim (E/E_S)^2$ and thus much relaxed experimental conditions. In this scenario relativistic electrons will be injected into the strong periodic field of an undulator or a laser. The resulting Lorentz-boost of the transversal field in the electron rest frame leads to an amplification of the electron acceleration. Whereas monoenergetic classical Larmor radiation with fixed polarization will be produced that exhibits a blind spot in acceleration direction, due to the Unruh effect photon pairs with opposite but otherwise arbitrary angular momentum direction will be created, obeying the resonance condition

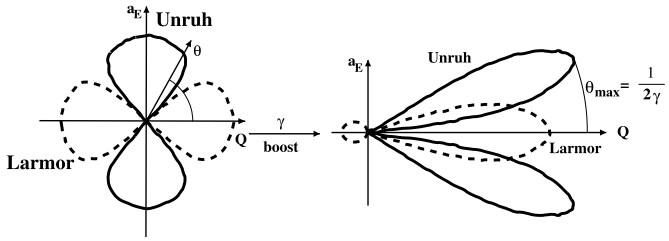

Fig. 3. Angular characteristics for Larmor and Unruh radiation before (left) and after the Lorentz boost (right). The acceleration direction by the electric field is indicated by a_E.

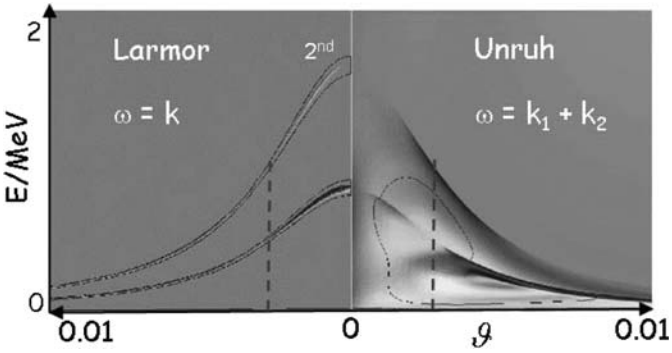

Fig. 4. Phase space for Larmor (left) and Unruh radiation (right) as calculated in the framework of non-linear QED [6].

$k_1 + k_2 = \omega = 2\gamma\omega_0$ (k_1, k_2: wave numbers of Unruh photons, ω: boosted optical frequency in the electron instantaneous rest frame). Thus Larmor and Unruh radiation can be distinguished according to their different energy and angular characteristics, as illustrated by the schematical picture of the angular characteristics shown in Figures 3 and 4, where the full phase space of Larmor (left) and Unruh radiation (right) is displayed as calculated in reference [6].

2.3 Experimental setup with an optical undulator

Figure 5 illustrates a possible experimental setup designed for the detection of Unruh photons generated in an experiment with oscillating electron acceleration. Using a TW (or PW) laser beam electrons can be accelerated in a gas-filled capillary (or from a thin diamond-like carbon foil) to energies around 150 MeV ($\gamma = 300$) with about 10^{10} electrons/bunch. These electrons are then injected into a counter-propagating linear or circular polarized second laser (ps pulse length, 10^{18} W/cm^2, $\hbar\omega_{\rm opt} \sim 2.5$ eV). In the instantaneous rest frame of the electrons this results for $E/E_S = 10^{-3}$ in a boosted optical frequency of 1.5 keV. As derived in reference [6], the emission probability for single Larmor photons from one electron after 100 laser cycles will result in $P_{\rm Larmor} \sim 10^{-1}$, while the corresponding emission probability for Unruh photon pairs amounts to $P_{\rm Unruh} = 4 \times 10^{-11}$. However, this at first glance rather unfavourable signal/background ratio can be improved by orders of magnitude when entering the regime of coherent emission exploiting a relativistic mirror. Moreover it should be noted that each electron bunch will typically contain about 10^{10} electrons which will be provided with the laser repetition frequency of presently 10 Hz. In addition, as illustrated in Figure 4, Larmor and Unruh photons strongly differ in energy and angular characteristics: while monoenergetic Larmor radiation with $\omega = k$ will be produced with an intensity minimum in acceleration direction ('blind spot'), Unruh photons obey the resonance condition $k_1 + k_2 \sim 500$ keV for the above given parameters and can thus be distinguished by suitable energy and angular filters. The accelerated electrons will be deflected and detected in a magnetic spectrometer (already existing at the MPQ), while photon detection will be performed in a position sensitive Compton spectrometer (see Sect. 3).

2.4 Experimental setup using a brilliant X-ray undulator

Presently novel experimental concepts have been studied, where brilliant γ and X-ray beams can coherently be produced via Compton backscattering off dense electron sheets used as relativistic mirrors [33].

The experimental scenario for the production of Unruh photons discussed above relied on relativistic electrons with $\gamma \sim 300$, interacting with an optical laser beam ($\hbar\omega_{0,1} \sim 2.5$ eV). In this situation the photon energy in the electron instantaneous rest frame amounts to $\hbar\omega_{int,1} = 2\gamma\,\hbar\omega_{0,1} = 1.5$ keV. These conditions result in the production of Unruh photons with a summed energy of about 900 keV.

Let us discuss now a scenario, where we aim at achieving a similar Unruh photon energy by using a significantly lower electron beam energy of e.g. 1 MeV ($\gamma = 2$). Such low-energy, yet monochromatic laser-accelerated electron beams can be realized using plasma density gradients in a gas jet decreasing in the laser propagation direction ('downramp'), thus allowing to control the wake phase velocity and trapping threshold in laser wakefield acceleration [27].

The resulting required primary photon energy $\hbar\omega_{0,2}$ amounts to about 20 keV. In this scenario an alternative experimental setup compared to Figure 5 could be realized by the schematics shown in Figure 6. Laser-accelerated low-energy electrons ($\gamma \sim 2$) interact with a brilliant X-ray beam produced from reflecting an optical laser beam off a relativistic dense electron sheet created by a driver laser focused onto a thin diamond-like carbon foil (DLC) with a thickness of typically 5 nm [33].

In the instantaneous rest frame of the electron this energy corresponds to $\hbar\omega_{int,2} = 2\gamma\hbar\omega_{0,2} = 80$ keV. Thus the ratio between the photon frequencies in the rest frame increases by a factor of $\hbar\omega_{int,2}/\hbar\omega_{int,1} = 53$ when using the X-ray beam instead of optical laser photons. Now we have to remind that the probability for the emission of a (single) Larmor photon can be expressed as [6]

$$\mathcal{P}^{1\gamma}_{\rm Larmor} = \alpha_{\rm QED} \left[\frac{qE}{m\omega}\right]^2 \mathcal{O}\left(\frac{\omega T}{2}\right) \qquad (4)$$

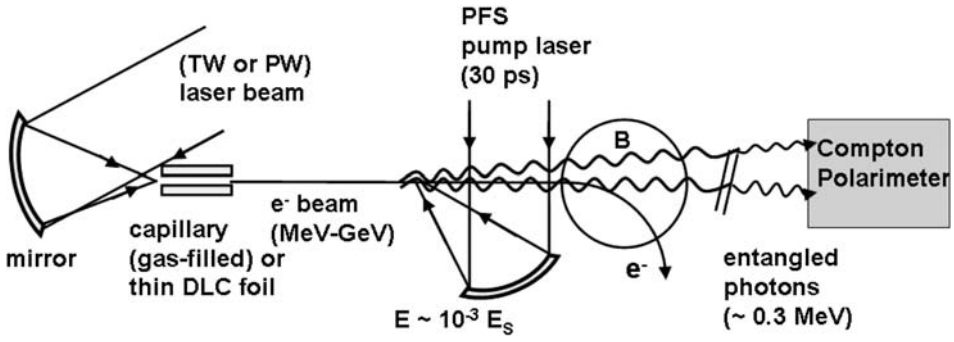

Fig. 5. Schematical view of an experimental setup for the detection of Unruh radiation originating from laser-accelerated energetic electrons interacting with the strong periodic field of a counter-propagating optical laser beam.

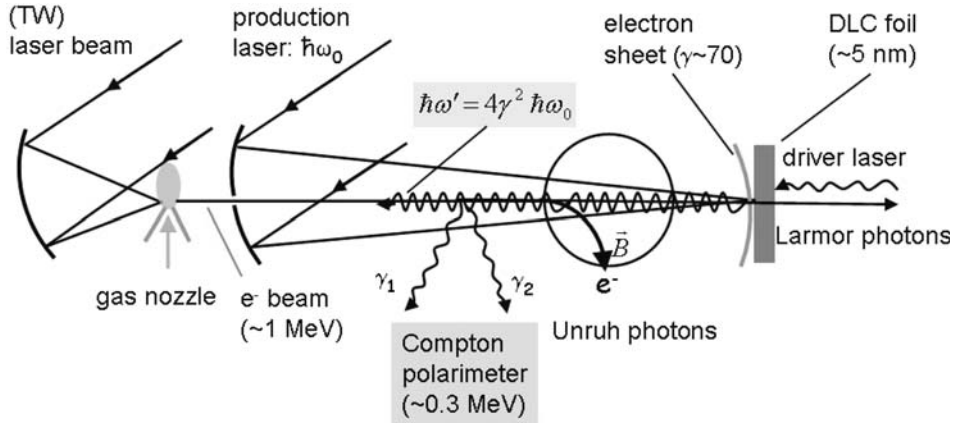

Fig. 6. Schematical view of an experimental setup for the detection of Unruh radiation originating from laser-accelerated low-energy electrons interacting with a brilliant X-ray beam produced from reflecting an optical laser beam off a relativistic dense electron sheet (see text) used as undulator.

while the corresponding probability for the creation of a pair of Unruh photons is given by

$$\mathcal{P}^{2\gamma}_{\text{Unruh}} = \frac{\alpha^2_{\text{QED}}}{4\pi}\left[\frac{E}{E_S}\right]^2 \mathcal{O}\left(\frac{\omega T}{30}\right). \qquad (5)$$

Thus the ratio between the emission probability for Unruh photon pairs and single Larmor photons is determined by the ratio $(\omega/m)^2$. Therefore it is evident that by increasing the undulator frequency in the rest frame of the electron from 1.5 keV to 80 keV the probability for the emission of (single) Larmor photons will be reduced by a factor of about 2.8×10^3, while the probability for the emission of Unruh photons remains unaffected. In addition the ratio between the electrical field strengths in the instantaneous rest frame of the electron in both scenarios differs by about a factor of 30 in favour of the X-ray undulator, therefore further increasing the gain factor by $(E_2^{int}/E_1^{int})^2 \sim 850$ to about 2.4×10^6. Whereas in the previous scenario with an optical undulator the resulting ratio between the emission of Unruh and Larmor photons resulted in $\mathcal{P}_{\text{Unruh}}/\mathcal{P}_{\text{Larmor}} = 4 \times 10^{-11}/10^{-1} = 4 \times 10^{-10}$, this ratio now improves to about 9.6×10^{-4}. Moreover, as discussed earlier, Unruh photons will always be created as (entangled) photon pairs, so for a realistic comparison of the emission probabilities of Unruh and Larmor photons also the two-photon Larmor emission probability has to be taken into account, given by the square of equation (4). The latter step strictly only holds for the case of a single accelerated electron, since in the usual situation of a large number of electrons per bunch the two Larmor photons will originate from different electrons. However, due to the clear signature of Unruh and Larmor photons in view of their spatial and energetic distribution as well as their polarization it seems justified to expect a significant improvement of the Unruh/Larmor ratio by detecting and analyzing Larmor photon pairs. Therefore the final ratio between the emission probabilities for Unruh and Larmor pairs improves in an optimistic scenario to the percent level of the Larmor radiation. Thus we can conclude that the choice of an X-ray undulator would drastically improve the possibility to discriminate Unruh photons from Larmor radiation background.

Table 2 lists a comparison of the relevant parameters for the two experimental scenarios discussed above. The first row shows the situation for the interaction of a fast electron beam ($\gamma = 300$) with an optical undulator (2×10^{15} photons with energy $\hbar\omega_0 = 2.5$ eV in 10 fs

Table 2. Comparison of relevant parameters given for the two experimental scenarios discussed in the text for the creation of Unruh photon pairs with a summed energy of 900 keV (320 keV) for the scenario listed in the top (bottom) row.

N_γ /bunch	$E_{kin,e}$ [MeV]	γ	I^{lab} [W/cm^2]	I^{int} [W/cm^2]	$\hbar\omega_0$ (*:$\hbar\omega'$) [eV]	$\hbar\omega_{int}$ [eV]	E^{lab} [V/m]	E^{int} [V/m]	a [g]	kT_U [eV]	hor. dist. d [m]
2×10^{15}	150	300	10^{18}	3.6×10^{23}	2.5	1.5×10^3	1.9×10^{12}	1.2×10^{15}	2.1×10^{25}	80	4×10^{-10}
10^{13}	1	2	2×10^{25}	3.2×10^{26}	2×10^4 *	8×10^4	8.7×10^{15}	3.5×10^{16}	6.2×10^{26}	2.2×10^3	1.5×10^{-11}

bunches), resulting in an Unruh temperature of 80 eV in the instantaneous rest frame of the electron, while in the laboratory frame Unruh photon pairs will be detectable with a sum energy of about 900 keV ($\hbar\omega_{int} = 2\gamma\hbar\omega_0$). A comparable situation can be realized using a 1 MeV electron beam interacting with X-ray undulator bunches each containing 10^{13} photons of 20 keV, focused to a diameter of 1 μm. In this case the electrical field strength in the electron instantaneous rest frame will already amount to $E^{int}/E_S = 0.027$ while producing a summed Unruh photon energy (in the laboratory frame) of about 320 keV.

Moreover, there are yet more advantages of this experimental scenario. Due to the small electron beam energy with $\gamma = 2$ the resulting Lorentz boost and hence the forward focusing of the produced γ radiation will be significantly reduced, ending in an emission cone of about $1/\gamma \approx 15°$ (compared to a much smaller angular segment with an opening of about 0.1° in case of $\gamma = 300$). Therefore the different emission characteristics between Larmor and Unruh radiation with the blind spot of Larmor radiation in acceleration direction can be exploited much more efficiently compared to the situation with $\gamma = 300$. For small values of γ the angular distribution of Larmor radiation will vary much less with θ compared to the situation illustrated in Figure 4, thus facilitating their discrimination from Unruh photons. Moreover, not only the spatial discrimination of the two radiation components will benefit from a lower electron beam energy, also the rather weak angular dependence of the energy characteristics in view of the broad emission cone of Unruh photons around the acceleration axis adds to the efficiency of discrimination from Larmor background.

From a practical point of view the photon detection in the low-γ scenario does not require any longer a very distant detector position because of the largely Lorentz-boosted emission cone, but instead the photon detector can be placed close to the interaction point, thus allowing for a coincident detection of both Unruh photons. Applying a polarization detection technique not only to individual photons but simultaneously to photon pairs allows to verify the opposite polarization of both photons that indicates their origin from the Unruh effect. In this way the Compton polarimeter introduced in the following section will be operated as a double-polarization spectrometer.

Focusing the 20 keV X-ray photons to about 1 μm, much less than the diffraction limit, will consequently allow for a large number of interactions with the 1 MeV electron bunch, which itself could be compressed by a counter-propagating laser beam used as electron bunch compressor via the light pressure force.

The theoretical description of the Unruh effect occurring as a result of non-uniform (here: periodic) acceleration as outlined in reference [6] is based on a quasi-classical treatment of the electrons. Hence the frequency ω_{int} of the external electromagnetic field E (measured in the rest frame of the electrons) lies far below the electron rest mass ($mc^2 \gg \hbar\omega_{int}$) and its normalized amplitude a is small ($qE \ll mc\omega_{int}$). This corresponds to the situation of a large value of the Keldysh adiabaticity parameter $\gamma = mc\omega_{int}/qE$ [2]. In our first experimental scenario with an optical undulator (2.5 eV) interacting with a fast electron beam ($\gamma = 300$) the (inverse) Keldysh parameter $qE/mc\omega_{int}$ amounts to 0.31, while for the second scenario with 20 keV X rays a value of 0.17 is obtained, both staying below unity as required for the perturbative regime.

With the normalized laser amplitude

$$a = eA/mc^2 = eE\lambda/(2\pi mc^2) \tag{6}$$

being a Lorentz invariant, relating to the laser intensity I and wavelength λ via $a^2 = I/1.37 \times 10^{18}$ [W/cm^2] $\times$ λ^2 [μm^2], a reduction of the wavelength by a factor of about 2×10^4 (as in the case of the 20 keV X-ray beam compared to a 1 eV optical undulator) while preserving $a < 1$ results in a drastic increase of I by about 4×10^8. Thus the electric field in this scenario will be very large ($E = \sqrt{I/(\epsilon_0 \times c)}$), which in turn results in an absolute increase of the emission probability $P_{\mathrm{Unruh}} \propto (E/E_S)^2$ besides the previously discussed suppression of competing Larmor background. Thus a sizable production rate of Unruh events of several 10^3 Unruh pairs per second could be achieved using electron bunches containing about 10^{10} electrons.

3 Identification of Unruh radiation via Compton polarimetry

Experimentally the generation of entangled photon pairs can be identified via Compton polarimetry, where a measurement of the azimuthal Compton scattering angle will be sensitive to the polarization of the detected photons [28].

3.1 Characteristics of Compton scattering

According to the kinematics of the Compton scattering process, i.e. the scattering of photons on free or quasi-free electrons, the energy of the scattered photon is given by

$$\hbar\omega' = \frac{\hbar\omega}{1 + \frac{\hbar\omega}{m_e c^2}(1 - \cos\theta)} \tag{7}$$

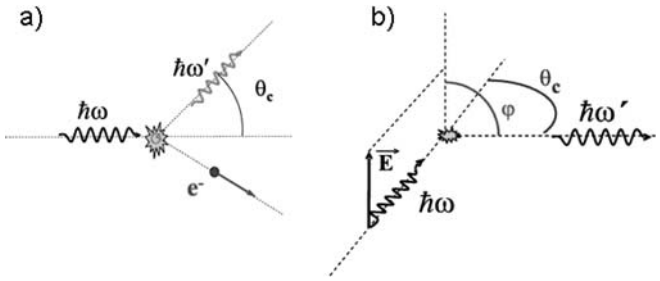

Fig. 7. (a) Kinematics of Compton scattering, (b) azimuthal Compton scattering angle ϕ relative to the polarization plane of the initial photon. Taken from reference [28].

here θ represents the Compton scattering angle, while $\hbar\omega$ and $\hbar\omega'$ correspond to the energy of the incident and scattered photon, respectively. Figure 7a illustrates the corresponding kinematics of the Compton scattering process, while in panel (b) the azimuthal scattering angle ϕ relative to the polarization plane of the incident photon is defined, which is the key observable for Compton polarimetry.

The angular dependence of the Compton scattering cross section is given by the Klein-Nishina equation [32]

$$\frac{d\sigma}{d\Omega} = \frac{r_0^2}{2}\,\frac{\hbar\omega'^2}{\hbar\omega^2}\left(\frac{\hbar\omega'}{\hbar\omega} + \frac{\hbar\omega}{\hbar\omega'} - 2\sin^2\theta\cos^2\phi\right) \quad (8)$$

with r_0 being the classical electron radius ($\sim$2.82 fm). This equation describes the sensitivity of Compton scattering to linear polarization.

As illustrated in Figure 8, two interaction points for scattering (X_1, Y_1) and absorption (X_2, Y_2) of the incoming γ ray ($E_\gamma = \hbar\omega$) define the azimuthal Compton scattering angle ϕ between the propagation direction of the scattered photon and the polarization vector of the incident photon (right panel). The differential Compton scattering cross section exhibits a characteristic angular dependency on ϕ with respect to the initial polarization vector **E** (left panel).

The scattering of linear polarized photons results in an azimuthal modulation of the detected photons, as seen in the left panel of Figure 8. The modulation fraction is defined by [29]

$$M(\phi) = \frac{N(\phi + 90°) - N(\phi)}{N(\phi + 90°) + N(\phi)} \quad (9)$$

with N denoting the angular dependent photon yield. M reaches its maximum when ϕ is in the direction of the incident polarization vector, while its minimum appears in the perpendicular direction. The modulation fraction is shown in Figure 9 as a function of the Compton scattering angle θ. Lower energies have a larger modulation fraction. The maximum modulation fraction of about 90% is achieved for energies below 200 keV and occurs for events where the Compton photon is scattered by about 90°. With increasing energy the peak slightly shifts to forward angles. The modulation fraction diminishes to zero for small scattering angle and in case of backscattering. Thus the most useful events for Compton polarimetry are those where photons are scattered into the limited regime of angles around 90°.

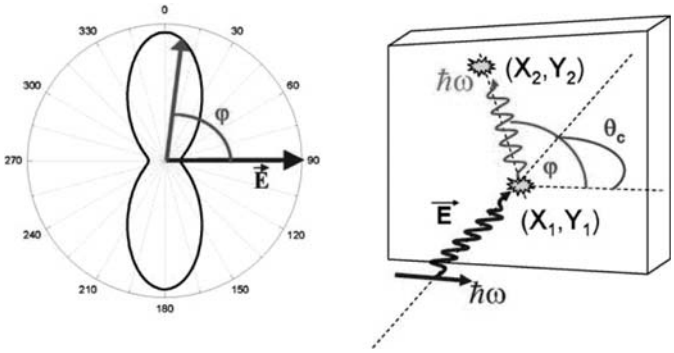

Fig. 8. Principle of Compton polarimetry. Left: differential cross section for Compton scattering. The ϕ distribution for a horizontally aligned photon polarization **E** is displayed. Right: definition of the azimuthal Compton scattering angle via the coordinates of the two interaction points for scattering (X_1, Y_1) and absorption (X_2, Y_2) of the incident horizontally polarized photon. Taken from reference [28].

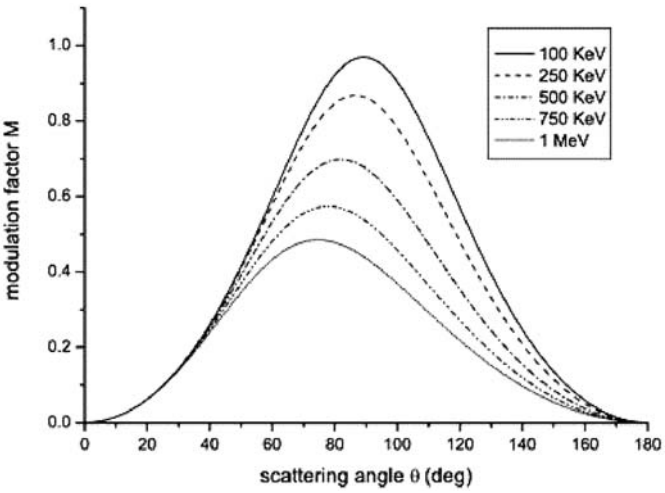

Fig. 9. Scattering angle dependence of the modulation fraction M for various photon energies. Taken from reference [28].

3.2 Compton polarimeter design considerations

In order to optimize the polarimeter, the product of the modulation fraction M and the Compton scattering cross section σ has to be considered, which is displayed in Figure 10 for three different photon energies. For the photon energy region below about 300 keV, relevant for our Unruh radiation studies, optimum polarization sensitivity is achieved in the scattering range between 70° and 90°.

The efficiency for Compton scattering and photoabsorption is the key parameter for the design of the Compton polarimeter. Therefore both Compton scattering and photoabsorption processes should have optimized cross sections for a given detector material. The top panel of Figure 11 compares the total absorption efficiencies for germanium and silicon crystals. In general germanium is more efficient as a photon absorber. In contrast, as shown in the bottom panel of Figure 11, where the contribution of the Compton scattering cross section to the total cross

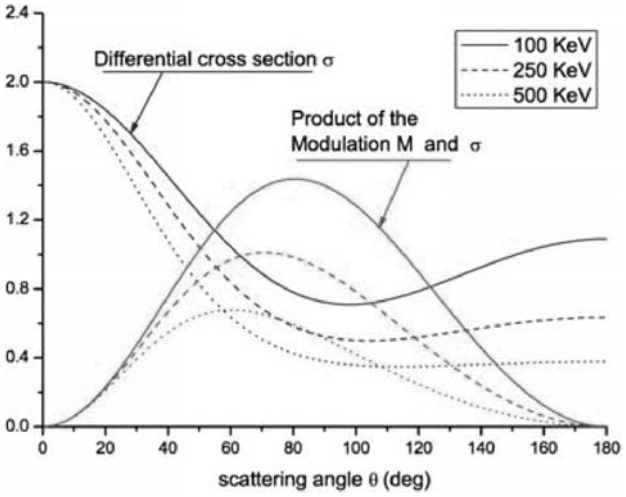

Fig. 10. Differential Compton scattering cross section and its product with the modulation fraction for 100% linearly polarized photons of different energies. Taken from reference [28].

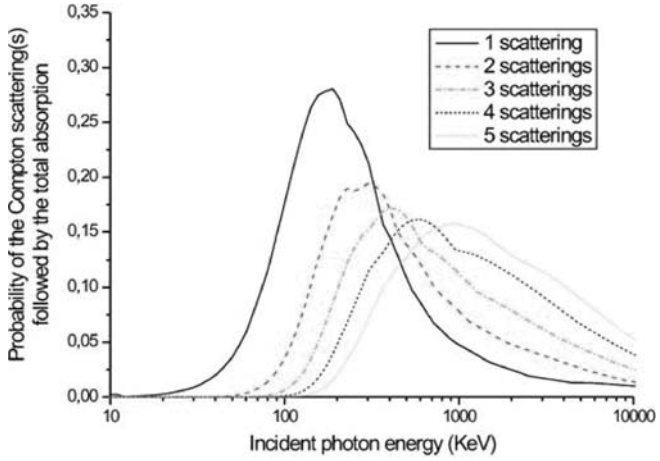

Fig. 12. Simulated multiple Compton scattering probability for a germanium crystal. 1–5 Compton scattering processes and subsequent photoabsorption have been calculated as a function of the incident photon energy. Taken from reference [28].

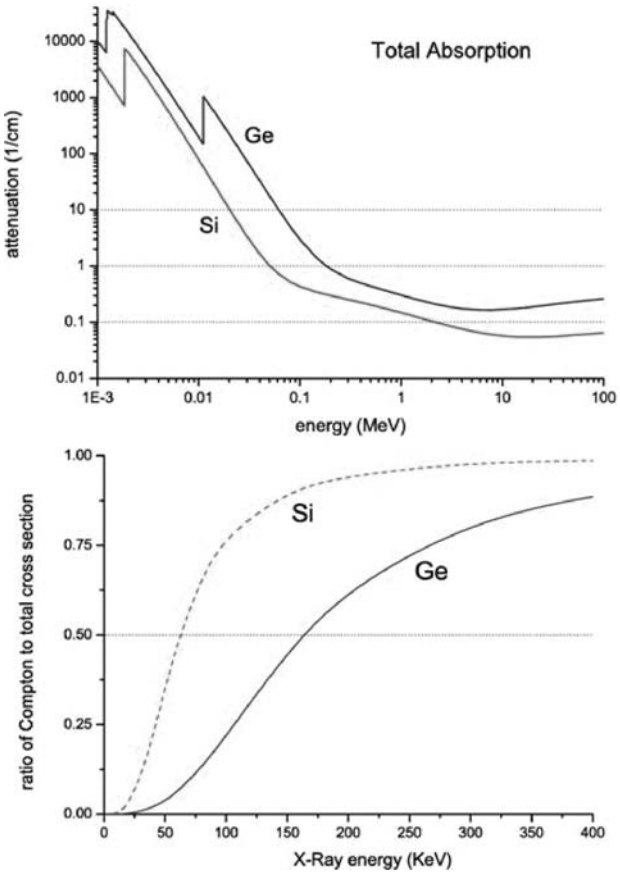

Fig. 11. Top: total photon absorption efficiencies for Ge and Si crystals. The absorption efficiency is given in terms of the attenuation coefficient. Bottom: contribution of the Compton scattering cross section to the total cross section of Ge and Si as a function of the incident photon energy. The level 0.5, where the Compton cross section is equal to the photo-absorption cross section indicates the energy region, where the optimum performance of the detector system can be achieved. Taken from reference [28].

section of Ge and Si is shown as a function of the photon energy, silicon exhibits a larger Compton scattering cross section. The horizontal line at 0.5, where the Compton cross section equals the photoabsorption cross section, indicates the energy region where the optimum performance of the detector system can be achieved. Obviously germanium is better suited than silicon for larger photon energies, here this optimum photon energy is about 160 keV, while for silicon it amounts only to about 60 keV. Therefore the Compton polarimeter presently under construction for the Unruh studies is based on germanium as detector material.

Furthermore it is important to note that in case of multiple Compton scattering events the information about the initial photon polarization will be lost typically after the second scattering. Therefore the detector design should be optimized for single Compton event detection. Figure 12 displays simulated probabilities for multiple scattering inside an infinite germanium crystal followed by photoabsorption [28]. With increasing photon energy the probability for multiple Compton scattering increases significantly. In order to restrict to predominantly single scattering events the incident photon energy should not exceed 300 keV.

The chosen granularity of a 2D-segmented polarimeter is a crucial design parameter, taking into account possible ambiguities from neighbouring pixels arising from e.g. charge sharing between adjacent strips or lateral diffusion of the charge cloud. Assuring unambiguous pattern detection requires isolated pixel hits, however at the cost of an efficiency reduction in the segmented detector. Thus in order to optimize the polarimeter, the detector has to have a rather fine granularity. On the other hand the detector dimensions must allow for an efficient detection of the Compton-scattered photon. Therefore the total detector thickness must be at least of the order of the absorption length. For the example of germanium, as chosen for the Unruh polarimeter, this value amounts to 17 mm for a photon energy of 300 keV, which will be about the energy

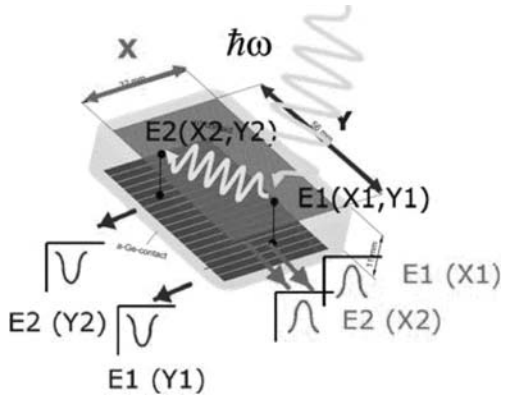

Fig. 13. Schematical illustration of the signals attainable from a 2D-segmented planar germanium detector. The position sensitivity allows for a precise localization of the scattering and absorption position of an incident photon.

range of interest for the Unruh photon studies. Moreover, in order to optimize the segmentation dimensions, it has to be taken into account that the probability for the occurrence of multiple hits within one pixel should be kept low, thus limiting the maximum strip size. On the other hand, the Compton scattered photons must be efficiently absorbed within a few pixels. As an empiric rule, the optimum segmentation size is 1/4 of the absorption length for a given photon energy [30]. Thus a segmentation width of 1 mm was chosen for the Unruh polarimeter.

3.3 2D-segmented Compton polarimeter

In order to realize the experimental setup for the identification of Unruh photons, an advanced position-sensitive planar germanium detector system based on the design considerations discussed in the previous section is presently under construction. The germanium detector crystal has a thickness of 20 mm with an active surface area of 80×80 mm^2. The front and back sides are segmented in 64 horizontal and vertical strips, respectively, each with a width of 1 mm. The high granularity allows to derive the position of the Compton scattering (X_1, Y_1) and photoabsorption (X_2, Y_2), as illustrated in Figure 13.

A photograph of a comparable detector operated at GSI [31] is shown in Figure 14.

An example for the quality of polarization sensitivity achievable with such a detector is shown in Figure 15. The spectrum displays the azimuthal intensity distribution of Compton scattered photons for 210 keV, linearly polarized incident photons [31]. The corresponding measurements have been performed with synchrotron radiation from the ESRF facility at Grenoble.

3.4 Experimental program

First experimental studies of the Unruh effect using laser-accelerated electron beams will be performed at the ATLAS laser facility of the MPI for Quantum Optics in

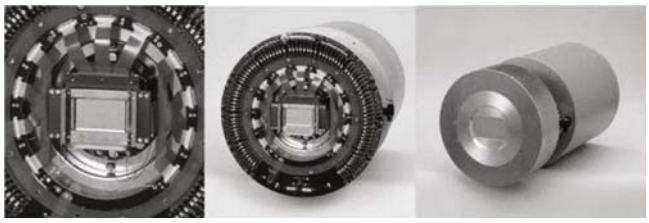

Fig. 14. Prototype of a 2D-segmented planar germanium Compton polarimeter as presently operated at GSI/Darmstadt [31]. A comparable detector with a design optimized for the detection of photons from Unruh (and Larmor) radiation with $E_\gamma < 300$ keV is presently under construction.

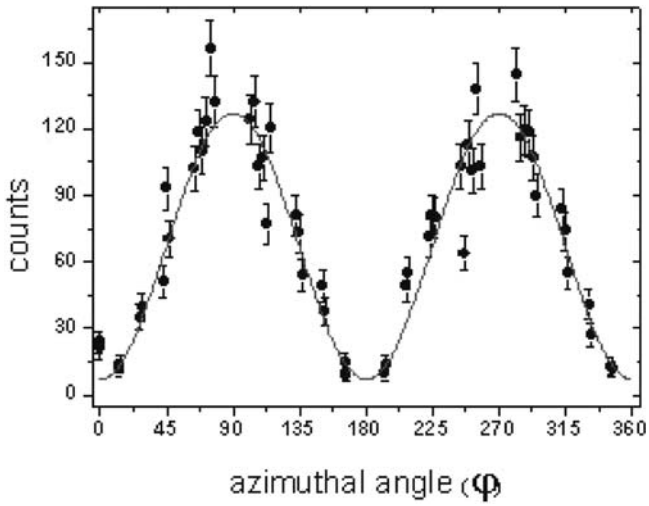

Fig. 15. Azimuthal intensity distribution of Compton-scattered photons for 210 keV, linear polarized incident photons [31].

Garching. Upon completion of an ongoing upgrade program, this laser system will be able to provide a laser power of 100 TW (pulse length: 30 fs, pulse energy: 3 J). Already at present laser accelerated electron beams with an energy of about 150 MeV can be routinely provided with excellent emittance.

In a first stage of the experiments the conditions for high-resolution γ spectroscopy in the vicinity of a pulsed high-power laser system have to be explored. Especially the requirements of electronic noise suppression and shielding of the sensitive spectroscopy electronics against the electromagnetic pulse (EMP) of the laser system may require specific experimental precautions (e.g. housing the detector and its electronics in a Faraday cage). Aiming at the experimental scenario using the X-ray undulator as outlined in Section 2.4, the Compton polarimeter can be positioned at an angle perpendicular to the laser propagation direction, close to the interaction region between electron bunch and X-ray beam, in this case optimized for the detection of entangled Unruh photon pairs. However, the first experimental step would be devoted to the first identification of the Larmor radiation component originating from linear acceleration. In this case the detector will have to be placed under 0°.

3.5 Perspectives with ELI

With the envisaged ELI laser system not only an ultimate laser power of about 1 EW with a repetition rate of 0.03/s can be achieved, but at a reduced power level of several hundreds of TW a much higher repetition rate up to the order of kHz will become available also for experiments on the Unruh effect. Investigating a weak effect like Unruh radiation will greatly benefit from an increase of count rate compared to present days' experiments running typically at 10 Hz.

Shielding requirements against the electromagnetic pulse (EMP) arising from the fast pulsing of the high laser power will become even more severe, forcing to electrically decouple the signal processing electronics from the laser environment via fibre optics. Moreover, a high pointing stability of the laser system will be required to secure the interaction overlap between the electron beam and the X-ray undulator beam. In an ultimate experimental setup one could imagine to arrange a barrel-like geometry of Compton polarimeter detectors around the interaction zone in order to maximize the detection efficiency.

4 Conclusion

In summary, an experimental identification of entangled photon pairs originating as a signature of the Unruh effect seems within reach, exploiting the ultra-high field regime accessible with present and next-generation high-power, short-pulse lasers. The most promising experimental scenario is given by using a brilliant 20 keV photon beam (created from coherent Compton backscattering off a relativistic dense electron sheet) in conjunction with a low-energy laser-accelerated electron beam ($\gamma \approx 2$). Using the X-ray beam as an undulator for the electrons will result in the creation of Unruh photon pairs well-separated in angle and energy from the main background contribution which is the classical Larmor radiation emitted by the linearly accelerated electrons. The identification of the Unruh radiation will be performed by Compton polarimetry, using a novel, highly granular 2D-segmented planar germanium spectrometer.

Even after turning aside all reference to the Unruh effect, the creation of these photon pairs is a pure quantum phenomenon and cannot be explained within classical electrodynamics. One frequently finds the statements that loop diagrams (in QED, for example) correspond to quantum effects whereas tree-level diagrams are classical. However, this notion is not always correct and the creation of the photon pairs under consideration provides a nice counter-example: even though it can be described by a tree-level Feynman diagram (to lowest order), this effect vanishes in the classical limit. Its main suppression is not given by the fine-structure constant α_{QED} but by the inverse of the electron mass $1/m$ (more precisely $\hbar\omega/mc^2$), cf. equations (4) and (5). The quantum nature of this creation process manifests itself in the entanglement of the photon pairs, for example, which can be measured with the described methods.

The authors acknowledge the support by the DFG Cluster of Excellence MAP (Munich-Centre for Advanced Photonics) and by the European Commission under contract ELI pp 212105 in the framework of the program FP7 Infrastructures-2007-1. R.S. acknowledges support from DFG under grant SCHU 1557/1 and C.M. acknowledges support from the Humboldt foundation.

References

1. F. Sauter, Z. Phys. **69**, 742 (1931); F. Sauter, Z. Phys. **73**, 547 (1931); W. Heisenberg, H. Euler, Z. Phys. **98**, 714 (1936); V. Weisskopf, Kong. Dans. Vid. Selsk., Mat.-fys. Medd. **XIV**, 6 (1936); J. Schwinger, Phys. Rev. **82**, 664 (1951)
2. R. Schützhold, H. Gies, G. Dunne, Phys. Rev. Lett. **101**, 130404 (2008)
3. W.G. Unruh, Phys. Rev. D **14**, 870 (1976)
4. S.W. Hawking, Commun. Math. Phys. **43**, 194 (1975)
5. R. Schützhold, G. Schaller, D. Habs, Phys. Rev. Lett. **97**, 121302 (2006)
6. R. Schützhold, G. Schaller, D. Habs, Phys. Rev. Lett. **100**, 091301 (2008)
7. W.G. Unruh, R.M. Wald, Phys. Rev. D **29**, 1047 (1984)
8. A. Higuchi, G.E.A. Matsas, D. Sudarsky, Phys. Rev. D **45**, R3308 (1992)
9. L.C.B. Crispino, A. Higuchi, G.E.A. Matsas, Rev. Mod. Phys. **80**, 787 (2008)
10. R. Schützhold, C. Maia, Eur. Phys. J. D **55**, 375 (2009)
11. J.S. Bell, J.M. Leinaas, Nucl. Phys. B **284**, 488 (1987)
12. W.G. Unruh, Phys. Rep. **307**, 163 (1998)
13. I. Freund, B.F. Levine, Phys. Rev. Lett. **23**, 854 (1969)
14. P. Eisenberger, S.L. McCall, Phys. Rev. Lett. **26**, 684 (1971)
15. Y. Yoda et al., J. Synchrotron Radiat. **5**, 980 (1998)
16. B. Adams et al., J. Synchrotron Radiat. **7**, 81 (2000)
17. P. Chen, T. Tajima, Phys. Rev. Lett. **83**, 256 (1999)
18. http://www.extreme-light-infrastructure.eu/
19. S.P.D. Mangles et al., Nature **431**, 535 (2004)
20. C.G.R. Geddes et al., Nature **431**, 538 (2004)
21. J. Faure et al., Nature **431**, 541 (2004)
22. W.P. Leemans et al., Nature Phys. **2**, 696 (2006)
23. S. Karsch et al., New J. Phys. **9**, 415 (2007)
24. Zs. Major et al., accepted for publication in: The Review of Laser Engineering (Journal of the Laser Society of Japan) (2009)
25. S. Gordienko et al., Phys. Rev. Lett. **94**, 103903 (2005)
26. P. Jacobs et al., Prog. Part. Nucl. Phys. **54**, 443 (2005)
27. C.G.R. Geddes et al., Phys. Rev. Lett. **100**, 215004 (2008)
28. S. Tashenov, Ph.D. thesis, Univ. Frankfurt, 2005, unpublished
29. A. Ferguson, Nucl. Instrum. Meth. **162**, 565 (1979)
30. R. Kroeger et al., Nucl. Instrum. Meth. A **436**, 165 (1999)
31. T. Stöhlker et al., J. Phys. **58**, 411 (2007)
32. J.D. Jackson, *Classical Electrodynamics*, 2nd edn. (Wiley, New York, 1975), p. 682
33. D. Habs et al., Appl. Phys. B **93**, 349 (2008)